Mean-field theory on a coupled system of ferromagnetism and electronic nematic order

Hiroyuki Yamase
Max-Planck-Institute for Solid State Research, D-70569 Stuttgart, Germany and
National Institute for Materials Science, Tsukuba 305-0047, Japan
(Received 17 December 2012; published 13 May 2013; publisher error corrected 17 May 2013)

We analyze an effective model on a square lattice with two types of forward scattering interactions, which, respectively, drive ferromagnetism (FM) and electronic nematic order via a d-wave Pomeranchuk instability (dPI). The FM and dPI in general compete with each other and they are typically separated by a first-order phase boundary in the plane of the chemical potential and temperature. Nevertheless, there is a parameter region where the dPI occurs inside the FM phase, leading to their coexistence. We also study the effect of a magnetic field by choosing a chemical potential where the ground state is paramagnetic without a field. In this case, instead of FM, the dPI competes with a metamagnetic instability. The latter occurs above a threshold strength of the FM interaction and otherwise the dPI is stabilized with a dome-shaped phase diagram in the plane of a magnetic field and temperature. The FM interaction shifts the center of the dome to a lower field, accompanied by a substantial reduction of the field range where the dPI is stabilized and by an extension of the first-order part of the transition line, although the maximal critical temperature does not change. Our results indicate that proximity to the FM instability can be important to understand the experimental phase diagram observed in the bilayer ruthenate $Sr_3Ru_2O_7$.

DOI: 10.1103/PhysRevB.87.195117 PACS number(s): 71.27.+a, 71.18.+y, 75.25.Dk, 74.70.Pq

I. INTRODUCTION

In the nematic liquid crystal,[1] rodlike molecules have a preferred orientation. This state is characterized by breaking of orientational symmetry, retaining other symmetries of the system. Electronic analogs of the nematic liquid crystal attract much interest. Electrons have spin and the direction is defined in spin space. Using spin degrees of freedom, a *spin* nematic state is studied in quantum spin systems.[2,3] Electrons also have orbital degrees of freedom. With orbital order such as an occupation difference between the d_{yz} and d_{zx} orbitals in a d-electron system, electrons may break orientational symmetry without any additional symmetry breaking, leading to an *orbital* nematic state.[4,5] Ferropnictides are possible materials for such a state.[6,7] On the other hand, the orientation can not be defined for charge itself. However, a nematic state can be realized by using a charge degree of freedom. Two routes toward a *charge* nematic state are proposed. When the system is close to a charge stripe order, namely one-dimensional charge order, where both translational and orientational symmetry are broken, fluctuations of charge stripes may restore the former but the latter may be still broken.[8] The charge nematic order can be obtained also without invoking charge stripes. It was found theoretically that the two-dimensional t-J (Ref. 9) and Hubbard (Ref. 10) models exhibit a tendency toward a d-wave Pomeranchuk[11] instability (dPI). In this state, the Fermi surface expands along the k_x direction and shrinks along the k_y direction, or vice versa, whereas in a real-space representation the nearest-neighbor hopping is effectively enhanced along one direction and suppressed along the other direction.

The dPI was extensively studied not only in the t-J (Refs. 9 and 12–14) and Hubbard (Refs. 10 and 15–19) models, but also in phenomenological models,[20,21] a model with central forces,[22,23] general Fermi-liquid schemes,[24,25] and continuum (not lattice) models.[26–31] Mean-field theory of the dPI (Refs. 20 and 21) showed that the dPI occurs around van Hove filling with a dome-shaped transition line. Typically, the transition is second order at high temperature and changes to first order at lower temperature. The end points of the second-order line are tricritical points. The mean-field phase diagram is characterized by a single energy scale in the weak-coupling limit, similar to the BCS theory of superconductivity, and thus various universal numbers were found.[21]

Fluctuations of the dPI suppress the first-order transition obtained in mean-field theory and when they are strong enough, the transition changes to be continuous even at zero temperature, leading to a quantum critical point.[32,33] At the quantum critical point, dPI fluctuations lead to a non-Fermi-liquid ground state.[34,35] At finite temperatures close to the dPI, thermal fluctuations become dominant. They turned out to truncate the original Fermi surface, leading to a Fermi-arc-like feature.[36]

Signatures of nematicity were observed in cuprate superconductors. Neutron scattering measurements revealed a strong anisotropy of magnetic excitations in momentum space.[37–39] The anisotropy showed strong temperature and doping dependencies, which are well captured in terms of the competition of the dPI and singlet pairing formation.[40,41] Transport measurements also revealed a very strong anisotropy of the Nernst coefficient,[42] which was interpreted as a signature of charge nematic order.[43]

There is growing evidence that the bilayer ruthenate $Sr_3Ru_2O_7$ (Sr327) exhibits a dPI in a strong magnetic field.[44–46] In fact, many features observed in experiments were well understood in terms of the dPI, for example, the metamagnetic transition,[47] the enhancement of the residual resistivity,[48] the bilayer effect,[49,50] the suppression of the critical temperature by impurities,[51] and the spin-orbit effect.[52] Furthermore, the experimental phase diagram is very similar to that obtained in mean-field theory.[53] In particular, it was found that the mean-field phase diagram is characterized by a single energy scale even in the presence of a magnetic field.[54] Therefore, there exist various universal ratios for a given chemical potential, which can be compared directly

with experimental data. Although several universal ratios agree with the experimental data, ratios of the characteristic temperature and field give one order of magnitude smaller than the experimental ones.[54]

This apparent inconsistency can not be resolved by invoking different choices of parameters. The key may lie in the set of experimental indications that Sr327 is located close to a ferromagnetic instability: a large Wilson ratio,[55] a uniaxial-pressure-induced ferromagnetic transition,[56] and the presence of ferromagnetic fluctuations observed by the inelastic neutron scattering,[57] the nuclear spin-lattice relaxation rate,[58] and thermal expansion measurements.[59] Moreover, several band calculations[60,61] for Sr327 (without a field) suggested that the system is close to ferromagnetism (FM). Hence, the presence of a ferromagnetic interaction is quite plausible in Sr327. In fact, several theoretical studies[62–64] for Sr327 focused on the role of ferromagnetic interactions, especially in the context of a metamagnetic transition observed in experiments.[65]

In this paper, we develop a mean-field theory by taking two types of forward scattering interactions, which drive the dPI and FM, respectively, into account. In the context of Sr327, it is interesting to explore how the mean-field phase diagram of the dPI obtained previously is modified by the presence of a ferromagnetic interaction and how well the experimental phase diagram of Sr327 is captured. Furthermore, the interplay of the dPI and FM is interesting in its own right. While FM is an instability in the spin channel whereas the dPI is in the charge channel, both are instabilities in the particle-hole channel of $\mathbf{q} = \mathbf{0}$ and do not break translational symmetry. Several theoretical analyses of microscopic models[52,66,67] actually suggested the presence of a ferromagnetic instability, which competes with the dPI. Therefore, in a more general setting we study the interplay of the dPI and FM, and clarify possible scenarios in such a coupled system.

We propose an effective model, suitable to address the interplay of the dPI and FM, and derive resulting phase diagrams. In Sec. II, we introduce a forward scattering model and present results in Sec. III by separating two cases: (i) zero magnetic field ($h = 0$) and (ii) finite magnetic field ($h \neq 0$). The latter case is relevant to Sr327. Conclusions follow in Sec. IV.

II. MODEL

To analyze a coupled system of the dPI and FM, we consider the following Hamiltonian on a square lattice:

$$\mathcal{H} = \mathcal{H}_0 + \mathcal{H}_\phi + \mathcal{H}_m + \mathcal{H}_Z. \tag{1}$$

The first term $\mathcal{H}_0$ is the kinetic term

$$\mathcal{H}_0 = \sum_{\mathbf{k}\sigma} (\epsilon^0_{\mathbf{k}} - \mu) c^\dagger_{\mathbf{k}\sigma} c_{\mathbf{k}\sigma}, \tag{2}$$

where $c^\dagger_{\mathbf{k}\sigma}$ ($c_{\mathbf{k}\sigma}$) is a creation (annihilation) operator of an electron with spin σ and momentum $\mathbf{k}$; μ is the chemical potential. The electron dispersion is given by

$$\epsilon^0_{\mathbf{k}} = -2t(\cos k_x + \cos k_y) - 4t' \cos k_x \cos k_y \tag{3}$$

with t and t' being the nearest- and second-nearest-neighbor hopping amplitudes, respectively.

The second term $\mathcal{H}_\phi$ is a forward scattering interaction driving a dPI,

$$\mathcal{H}_\phi = -\frac{g_\phi}{2N} \sum_{\mathbf{k}\mathbf{k}'\sigma\sigma'} d_{\mathbf{k}} d_{\mathbf{k}'} c^\dagger_{\mathbf{k}\sigma} c_{\mathbf{k}\sigma} c^\dagger_{\mathbf{k}'\sigma'} c_{\mathbf{k}'\sigma'}, \tag{4}$$

where the coupling constant g_ϕ is positive, $d_{\mathbf{k}}$ is a d-wave form factor such as $d_{\mathbf{k}} = \cos k_x - \cos k_y$, and N is the total number of lattice sites. This term describes the d-wave weighted density-density interaction with zero momentum transfer, which was obtained in microscopic models such as the t-J (Ref. 9) and Hubbard (Refs. 10 and 66) models.

The third term $\mathcal{H}_m$ describes an Ising ferromagnetic interaction

$$\mathcal{H}_m = -\frac{g_m}{2N} \sum_{\substack{\mathbf{k}\mathbf{k}' \\ \sigma\sigma'}} \left(c^\dagger_{\mathbf{k}\sigma} \frac{\sigma}{2} c_{\mathbf{k}\sigma} \right) \left(c^\dagger_{\mathbf{k}'\sigma'} \frac{\sigma'}{2} c_{\mathbf{k}'\sigma'} \right), \tag{5}$$

where $g_m(>0)$ is a coupling constant and $\sigma = +1$ and -1 for up spin and down spin, respectively. This interaction is obtained by focusing on the spin-spin interaction with a spin quantization axis parallel to the z direction and by extracting a scattering process with zero momentum transfer. Therefore, the interaction described by $\mathcal{H}_m$ is appropriate when the system has a strong spin anisotropy as well as dominant forward scattering processes of electrons. The interaction of $\mathcal{H}_m$ is also obtained by considering a mean-field analysis of spin rotational invariant interactions. For instance, in the case of the Hubbard onsite interaction $U \sum_i n_{i\uparrow} n_{i\downarrow}$, our coupling constant is given by $g_m = 2U$.

The last term $\mathcal{H}_Z$ is the Zeeman energy

$$\mathcal{H}_Z = -\frac{h}{2} \sum_{\mathbf{k}\sigma} \sigma c^\dagger_{\mathbf{k}\sigma} c_{\mathbf{k}\sigma}. \tag{6}$$

Here, h is an effective magnetic field given by $h = \mathfrak{g}\mu_B H$, with $\mathfrak{g}$ being a g factor, μ_B is the Bohr magneton, and H is a magnetic field.

Our Hamiltonian (1) can be considered as an effective model at a low-energy scale, where two different interactions, each of which drives the dPI and FM, respectively, become dominant. The terms of $\mathcal{H}_\phi$ and $\mathcal{H}_m$ describe pure forward scattering interactions of electrons. Thus, fluctuations around the mean field vanish in the thermodynamic limit. In other words, mean-field theory solves our Hamiltonian exactly in the limit of $N \to \infty$.

The order parameter of the dPI is defined by

$$\phi = \frac{g_\phi}{N} \sum_{\mathbf{k}\sigma} d_{\mathbf{k}} \langle c^\dagger_{\mathbf{k}\sigma} c_{\mathbf{k}\sigma} \rangle. \tag{7}$$

This quantity becomes finite only if the system breaks square lattice symmetry because of the presence of the d-wave form factor. FM order is defined by

$$m = \frac{g_m}{2N} \sum_{\mathbf{k}\sigma} \sigma \langle c^\dagger_{\mathbf{k}\sigma} c_{\mathbf{k}\sigma} \rangle, \tag{8}$$

where we include the coupling constant g_m in the definition of m; while the magnetization is then given by m/g_m, we may refer to m as magnetization, as long as no confusion occurs. We decouple the interaction terms (4) and (5) by introducing

the order parameters ϕ and m, and obtain the mean-field Hamiltonian

$$\mathcal{H}_{\rm MF} = \sum_{\mathbf{k}\sigma} \xi_{\mathbf{k}\sigma} c^{\dagger}_{\mathbf{k}\sigma} c_{\mathbf{k}\sigma} + \frac{N}{2g_m} m^2 + \frac{N}{2g_\phi}\phi^2, \tag{9}$$

where the renormalized dispersion is given by

$$\xi_{\mathbf{k}\sigma} = \epsilon^0_{\mathbf{k}} - \frac{\sigma}{2}(m+h) - d_{\mathbf{k}}\phi - \mu. \tag{10}$$

The grand canonical potential per site at temperature T is obtained as

$$\omega = -\frac{T}{N}\sum_{\mathbf{k}\sigma} \ln(1 + e^{-\xi_{\mathbf{k}\sigma}/T}) + \frac{1}{2g_m} m^2 + \frac{1}{2g_\phi}\phi^2. \tag{11}$$

The stationary condition of ω with respect to ϕ and m leads to the self-consistent equations

$$\phi = \frac{g_\phi}{N}\sum_{\mathbf{k}\sigma} d_{\mathbf{k}} f(\xi_{\mathbf{k}\sigma}), \tag{12}$$

$$m = \frac{g_m}{2N}\sum_{\mathbf{k}\sigma} \sigma f(\xi_{\mathbf{k}\sigma}), \tag{13}$$

which we solve numerically. Here, $f(\xi_{\mathbf{k}\sigma})$ is the Fermi function.

III. RESULTS

We fix $g_\phi/t = 1$ throughout this paper unless otherwise noted and explore how the phase diagram of the dPI changes with increasing the FM interaction g_m. We first study the case of $h = 0$ and then that of $h \neq 0$. As a band parameter, we choose $t'/t = 0.35$, which was used for the study of Sr327.[53,54] Since the presence of t' turns out to play a crucial role to understand phase diagrams for $h = 0$, we also study the case of $t' = 0$ for $h = 0$. Hereafter, we set $t = 1$ and all quantities with dimension of energy are in units of t.

A. Results for $h = 0$

1. Evolution of phase diagrams with increasing FM interaction

Figure 1 shows a sequence of phase diagrams for $g_m \leqslant 7.0$ in the plane of the chemical potential μ and temperature T. Because of the competition with the dPI, no FM instability occurs at least up to $g_m = 6.0$ [Fig. 1(a)] and the phase diagram is occupied only by the dPI. As already clarified previously,[20,21] the dPI occurs below a dome-shaped transition line, with a maximal T_c near the van Hove energy ($\mu_{\rm vH} = 4t' = 1.4$); a deviation from $\mu_{\rm vH}$ is due to the presence of t', which breaks particle-hole symmetry. The phase transition is of second order at high temperature ($T_c^{\rm 2nd}$) and of first order at low temperature ($T_c^{\rm 1st}$). The end points of the second order line are tricritical points ($T_c^{\rm tri}$).

For $g_m = 6.5$, the FM interaction becomes strong enough to realize FM near the edge on the side of a high chemical potential [Fig. 1(b)]. The transition from the paramagnetic to FM phase is second order at high temperature, but the second-order line ends at a tricritical point and changes to a first-order line at low temperature. This feature is the same as the transition between the paramagnetic and dPI phases. The boundary of the dPI and FM is characterized by a first-order transition ($T_{\phi m}^{\rm 1st}$).

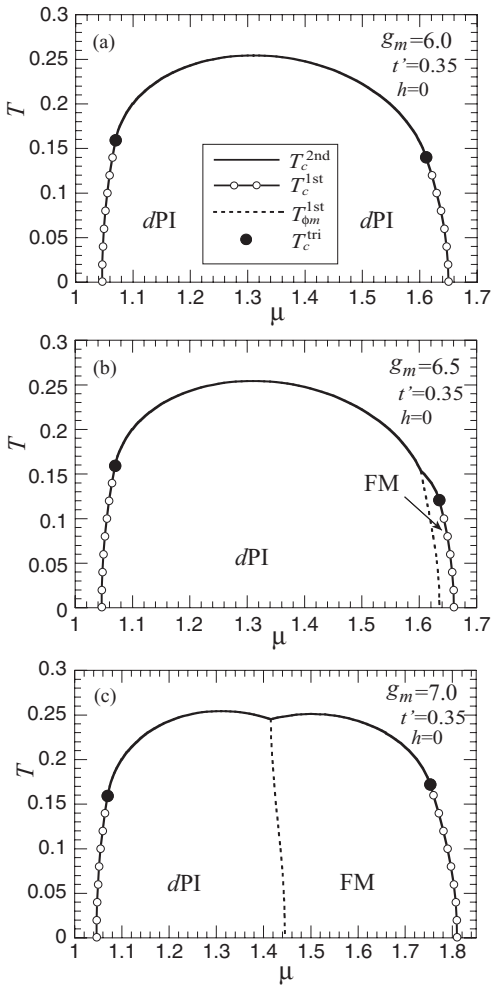

FIG. 1. Phase diagram in the (μ,T) plane for a sequence of couplings g_m. Transition from the paramagnetic to ordered phase is a second order ($T_c^{\rm 2nd}$) at high T and a first order ($T_c^{\rm 1st}$) at low T; $T_c^{\rm tri}$ is the temperature at a tricritical point. A dashed line ($T_{\phi m}^{\rm 1st}$) denotes the first-order phase boundary between the dPI and FM, which appears in (b) and (c).

As shown in Fig. 1(c), this first-order phase boundary shifts to the middle of the phase diagram for $g_m = 7.0$ and the FM becomes more stable. The order parameters are plotted as a function of μ in Figs. 2(a) and 2(b) at $T = 0.01$ and 0.20, respectively. At a low temperature ($T = 0.01$), ϕ and m show a jump at $\mu \approx 1.05$ and 1.81, respectively, because of a first-order transition from the paramagnetic phase. The dPI changes to the FM via a first-order transition at $\mu \approx 1.45$ and there is no mixing of ϕ and m. At a high temperature ($T = 0.20$), on the other hand, ϕ and m develop continuously at $\mu \approx 1.10$ and 1.72, respectively. The transition between the dPI and FM is, however, still of first order.

As expected, with further increasing g_m, the first-order boundary between the dPI and FM shifts to a lower chemical potential. In fact, as shown in Fig. 3(a), the dPI is realized only near the edge of the dome for $g_m = 7.8$. However, qualitative changes occur in the phase diagram. First, the coexistence of the dPI and FM is stabilized inside the FM phase near the edge of the first-order line of the FM around $\mu = 2.04$. This region is magnified in Fig. 3(b). The transition from the

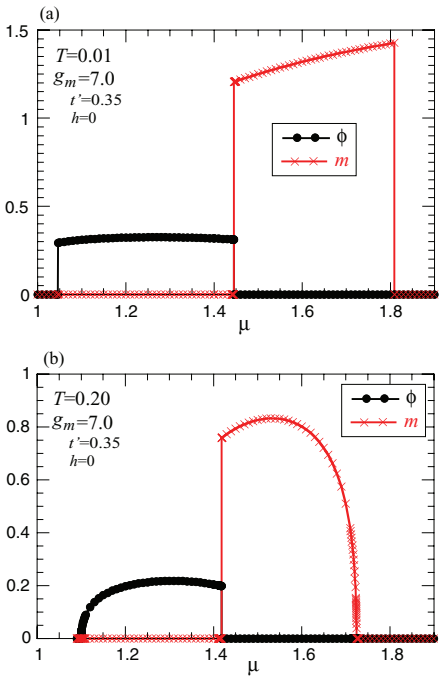

FIG. 2. (Color online) μ dependence of ϕ and m at $T = 0.01$ (a) and 0.20 (b) for $g_m = 7.0$.

FM to the coexistence is first order at low temperature and becomes second order at high temperature. While one end point of the second-order line at $\mu \approx 2.037$ is a tricritical point, the other end point at $\mu \approx 2.045$ is just a point touching the first-order line of the FM. There is a direct first-order transition from the paramagnetic phase to the coexistence around $\mu = 2.05$. Second, an additional FM phase appears in $2.52 \lesssim \mu \leqslant 2.6$ as shown in Figs. 3(a) and 3(c). This FM comes from the enhancement of the density of state at the band edge of $\mu = 2.6$. A first-order transition occurs only on the side of a lower chemical potential and the second-order line

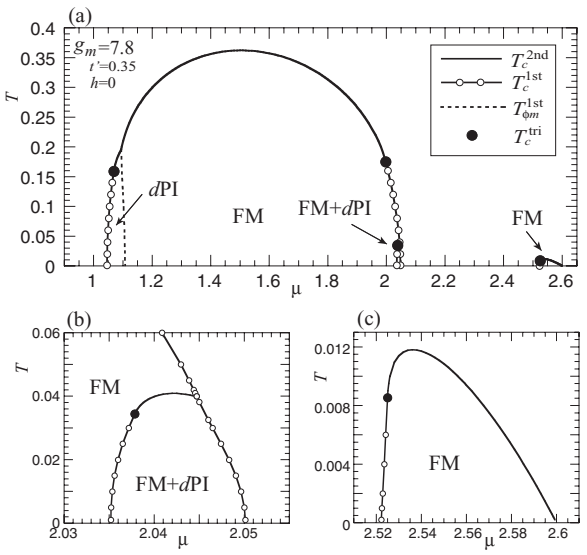

FIG. 3. Phase diagram in the (μ, T) plane for $g_m = 7.8$. The regions near $\mu = 2.04$ and 2.55 are magnified in (b) and (c), respectively.

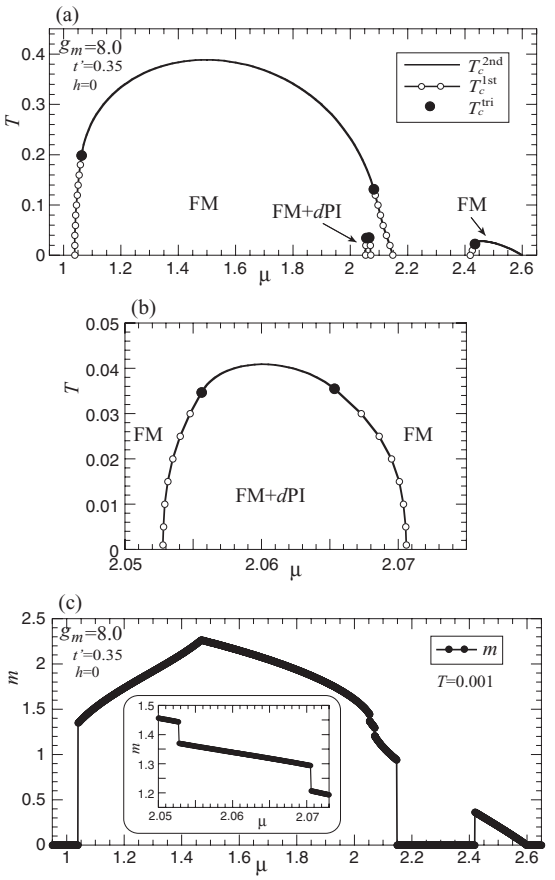

FIG. 4. (a) Phase diagram in the (μ, T) plane for $g_m = 8.0$. The region of the coexistence around $\mu = 2.06$ is magnified in (b). (c) μ dependence of m at $T = 0.001$. Two successive jumps around $\mu = 2.06$ are magnified in the inset.

disappears at the band edge. This band-edge FM is realized for $7.6 \lesssim g_m \lesssim 8.0$.

For $g_m = 8$, as shown in Fig. 4(a), the FM becomes dominant and a pure dPI phase is not stabilized. Instead, the dPI is realized in coexistence with the FM around $\mu = 2.06$, as magnified in Fig. 4(b). In contrast to the case of $g_m = 7.8$ [Fig. 3(b)], the phase boundary of the coexistence is well separated from the first-order line of the FM, leading to a phase diagram very similar to that of the pure dPI [Fig. 1(a)], but with a significant extension of the first-order portion of the transition line; the reason for this will be explained later in terms of Eq. (21). The magnetization m is plotted as a function of μ in Fig. 4(c) at low temperature. After the first-order FM transition at $\mu \approx 1.05$, the value of m increases with increasing μ and forms a cusp at $\mu \approx 1.45$ where the density of states of up-spin electrons is fully occupied and the system changes to a half-metallic state. For $\mu \gtrsim 1.45$, m decreases since electrons with down spin increase whereas the electron density of up spin remains unity. At $\mu \approx 2.05$ and 2.07, m exhibits a jump [see the inset of Fig. 4(c)] because of the presence of the coexistence of the dPI and FM, which occurs via a first-order transition at low T. The magnetization m vanishes discontinuously at $\mu \approx 2.15$, but appears again with a jump at $\mu \approx 2.42$ because of a first-order transition associated with the band-edge FM. The magnitude of m decreases monotonically and vanishes

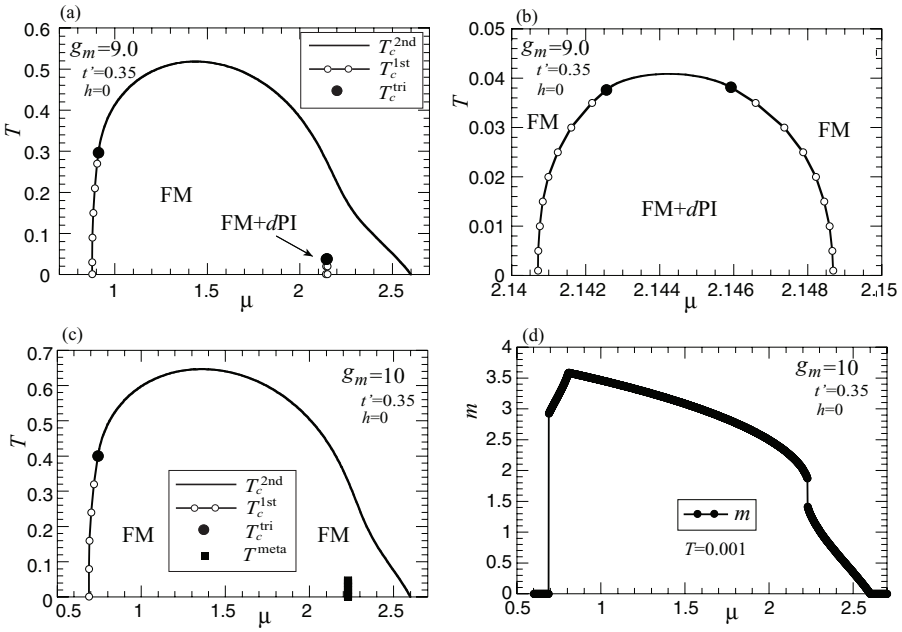

FIG. 5. (a) Phase diagram in the (μ,T) plane for $g_m = 9.0$. The region of the coexistence is magnified in (b). (c) Phase diagram for $g_m = 10$. $T^{\rm meta}$ denotes the position where a metamagnetic transition occurs. (d) μ dependence of m at $T = 0.001$ for $g_m = 10$.

at the band edge of $\mu = 2.6$. The system becomes a band insulator for $\mu > 2.6$.

With further increasing g_m (Fig. 5), the band-edge FM is absorbed into the main FM phase. A first-order phase transition then occurs only on the lower side of μ. Inside the FM, the coexistence of the dPI and FM is stabilized up to $g_m = 9.8$. Figure 5(a) is the representative phase diagram computed for $g_m = 9$. In Fig. 5(b), the region of the coexistence of the dPI and FM is magnified. This phase diagram is very similar to that for $g_m = 8$ [Fig. 4(b)] with the same maximal T_c, but with a further extension of the first-order transition line. For $g_m \gtrsim 9.8$, however, the coexistence is replaced by a first-order transition associated with a jump of the magnetization, namely, a metamagnetic transition inside the FM, as denoted by solid squares in Fig. 5(c). The magnetization is potted as a function of μ at low T in Fig. 5(d). The jump at $\mu \approx 2.23$ comes from the metamagnetic transition. The cusp at $\mu \approx 0.81$ indicates that the up-spin band is fully occupied in $\mu \gtrsim 0.81$, where the system becomes half-metallic.

2. Discussions

The coexistence of the dPI and FM is stabilized even for $g_m \gg g_\phi$ (Figs. 3–5). This is because of the presence of the van Hove singularity. After performing explicit calculations up to $g_m = 10$, we confirm the van Hove singularity due to the down-spin band ($m > 0$ is assumed) inside the FM phase for $g_m \gtrsim 7.8$. Around the van Hove filling, either the dPI or a metamagnetic transition occurs in our model, depending on energetics. We find that the coexistence of the dPI and FM is more favorable for $7.8 \lesssim g_m \lesssim 9.8$ and the metamagnetic transition for $g_m \gtrsim 9.8$.

The results shown in Figs. 1–5 are very asymmetric with respect to the van Hove energy of the bare dispersion, which is given by $\mu_{\rm vH} = 4t' = 1.4$. This is because the presence of t' breaks particle-hole symmetry. In fact, for $t' = 0$, the phase diagram becomes symmetric with respect to the axis of $\mu = 0$. For $0 \leqslant g_m \leqslant 8.84$, the dPI is stabilized and no FM is realized [Fig. 6(a)]. For $g_m \gtrsim 8.85$, however, the dPI starts to be replaced by the FM phase from a higher temperature [Fig. 6(b)] and is stabilized only around $\mu = 0$ at low T for $g_m = 8.86$ [Fig. 6(c)]. The dPI disappears already for $g_m = 8.87$. The change from the dPI [Fig. 6(a)] to the FM phase [Fig. 6(d)] occurs in a very small range of g_m. In contrast to the case of Figs. 3–5, no coexistence of the dPI and FM is stabilized. Furthermore, a band-edge FM does not appear.

Our results for $h = 0$ are summarized as follows: (i) in $0 \leqslant g_m \leqslant g_{m1}$, only the dPI phase is realized, (ii) in $g_{m1} \leqslant g_m \leqslant g_{m3}$, both dPI and FM are stabilized, but they are separated from each other by a first-order transition line, (iii) in $g_{m2} \leqslant g_m \leqslant g_{m4}$, the coexistence with dPI occurs inside the FM phase, and (iv) in $g_{m4} \leqslant g_m$, only the FM is realized. We have obtained $g_{m1} \approx 6.5$, $g_{m2} \approx 7.8$, $g_{m3} \approx 7.9$, and $g_{m4} \approx 9.8$ for $t' = 0.35$, leading to rich phase diagrams as shown in Figs. 1 and 3–5. For $t' = 0$, on the other hand, we have obtained $g_{m1} \approx 8.84$, $g_{m2} = g_{m3} = g_{m4} \approx 8.87$. As a result, a phase diagram is occupied by either the dPI or FM except for a tiny range of g_m.

B. Results for $h \neq 0$

Next, we examine the effect of a magnetic field, motivated by the experimental indication that Sr327 is paramagnetic in zero field and exhibits a nematic instability around 8 T.[44–46] Fixing the chemical potential $\mu = 1$ and taking the field as a tuning parameter, we study how the phase diagram of the dPI evolves with increasing the ferromagnetic interaction.

Figure 7(a) is a set of phase diagrams of the dPI in the plane of a magnetic field and temperature for a sequence of g_m, showing four characteristic features: with increasing g_m, (i) the dPI occurs in a lower field, (ii) the field range where the dPI is stabilized shrinks substantially, (iii) the first-order part of the transition line extends and tricritical points are pushed up to higher temperatures, but (iv) the maximal T_c does not change.

To understand these features, we consider a magnetic field $h_{\rm vH}$, at which the σ-spin band touches the van Hove energy,

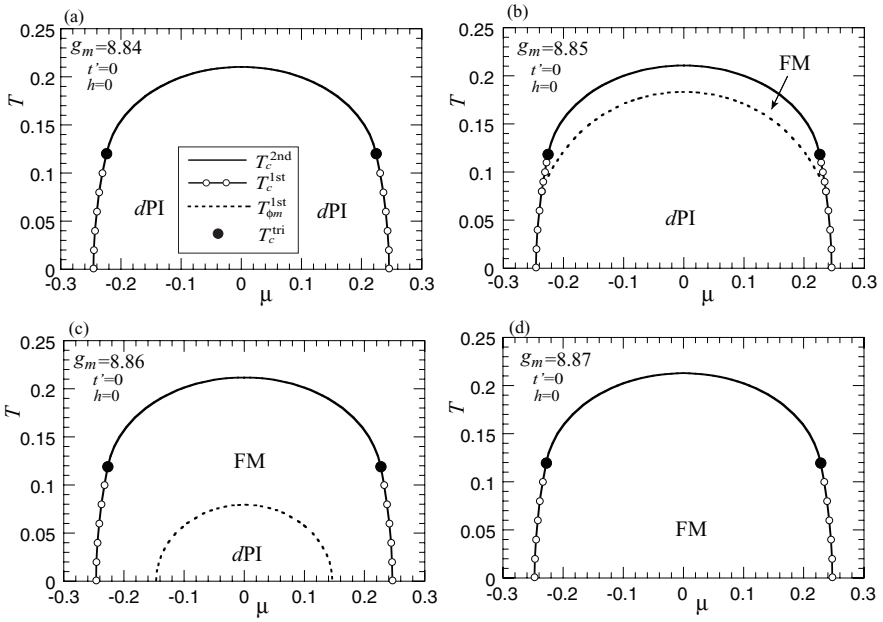

FIG. 6. Phase diagram in the (μ,T) plane for a sequence of couplings g_m by setting $t'=0$. The phase diagram is occupied by the dPI in $g_m \leqslant 8.84$ (a) and by the FM in $g_m \geqslant 8.87$ (d). In a tiny range of g_m [(b) and (c)], both FM and dPI are realized, but separated from each other by a first-order boundary; the line of $T_{\phi m}^{1st}$ appears only in (b) and (c).

and the dPI is expected around that. From Eq. (10), $h_{\rm vH}$ fulfills for $\phi=0$ the relation

$$\frac{\sigma(m+h_{\rm vH})}{2}+\mu=\mu_{\rm vH}, \tag{14}$$

and the corresponding relation for the other spin band should be $-\sigma(m+h_{\rm vH})/2+\mu=2\mu-\mu_{\rm vH}$, where $\mu_{\rm vH}=4t'$. Since μ is fixed in our case, we obtain

$$h_{\rm vH}=2|\mu-\mu_{\rm vH}|-m. \tag{15}$$

While the magnetization is not fully linear in field in the entire field range we consider, we may invoke the equation obtained in linear response theory

$$m/g_m \approx \chi h_{\rm vH} \tag{16}$$

$$=\frac{\chi_0}{1-g_m\chi_0}h_{\rm vH}, \tag{17}$$

where χ is the full magnetic susceptibility, which is expressed by the noninteracting magnetic susceptibility χ_0 as shown in the second line; the presence of g_m on the left-hand side is due to our definition of m [see Eq. (8)]. We then obtain

$$h_{\rm vH}=2(1-g_m\chi_0)|\mu-\mu_{\rm vH}|, \tag{18}$$

that is, the value of $h_{\rm vH}$ is reduced with increasing g_m. Since the dPI occurs around the van Hove energy, the dPI should be realized around a lower field with increasing g_m.

Equation (16) is a rough approximation especially near a metamagnetic transition and the resulting Eq. (18) should be taken as qualitative understanding. To get quantitative understanding, we solve Eq. (13) numerically under the condition of $\phi=0$ and Eq. (14). We then obtain $h_{\rm vH}\approx 0.61,0.41,0.22,0.12$ for $g_m=2,4,6,7$, respectively; for $g_m=0$, on the other hand, $h_{\rm vH}=2|\mu_{\rm vH}-\mu|=0.8$ since $m=0$. The dPI indeed occurs around those fields in Fig. 7.

The range of a magnetic field where the dPI is stabilized becomes narrower for a larger g_m. As seen in Eq. (10), the sum of m and h plays a role as an effective field. Since m becomes more susceptible to a field as g_m becomes larger and furthermore m is proportional to g_m in our definition [Eq. (8)], the value of h to stabilize the dPI is necessarily reduced.

The first-order transition line extends with increasing g_m. To understand this, we expand the free energy Eq. (11) with respect to the order parameter of the dPI around $\phi=0$,

$$\omega(\phi;m)-\omega(0;m)=\frac{1}{2}a_2\phi^2+\frac{1}{4!}a_4\phi^4+\cdots. \tag{19}$$

The coefficients of a_2 and a_4 are obtained as

$$a_2=\frac{1}{g_\phi}\left(1+\frac{g_\phi}{N}\sum_{\mathbf{k}\sigma}d_{\mathbf{k}}^2 f'\left(\xi_{\mathbf{k}\sigma}^0\right)\right), \tag{20}$$

$$a_4=\frac{1}{N}\sum_{\mathbf{k}\sigma}d_{\mathbf{k}}^4 f'''\left(\xi_{\mathbf{k}\sigma}^0\right)-3g_m\frac{\left[\frac{1}{2N}\sum_{\mathbf{k}\sigma}\sigma d_{\mathbf{k}}^2 f''\left(\xi_{\mathbf{k}\sigma}^0\right)\right]^2}{1+\frac{g_m}{4N}\sum_{\mathbf{k}\sigma}f'\left(\xi_{\mathbf{k}\sigma}^0\right)}, \tag{21}$$

where $\xi_{\mathbf{k}\sigma}^0=\epsilon_{\mathbf{k}}^0-\frac{\sigma(m+h)}{2}-\mu$ and f',f'',f''' are the first, second, third derivatives of the Fermi function. When a_4 becomes negative, a first-order transition can occur. The second term on the right-hand side of Eq. (21) originates from the ϕ dependence of m. The denominator of this term is positive close to the dPI and the numerator becomes in general finite when the spin symmetry is broken. Hence, the second term is negative for $h\neq 0$. Furthermore, the second term is proportional to g_m. Therefore, the presence of the second term in Eq. (21) leads to an extension of the first-order transition line of the dPI and this effect becomes stronger for a larger g_m. The same argument explains the extension of the first-order portion of the transition line in Figs. 4(b) and 5(b) since the second term of Eq. (21) becomes negative also in the FM phase.

A second-order transition is given by the condition $a_2=0$. Since μ is fixed, the quadratic term a_2 is a function of $\tilde{h}=m+h$. Suppose the maximal T_c is obtained at $\tilde{h}_{\rm max}$, there can exist a field h and a magnetization m, which give the same value of $\tilde{h}_{\rm max}$ for a different g_m, although the values of m and h themselves depend on g_m. This is actually the case up to $g_m=7.8$,

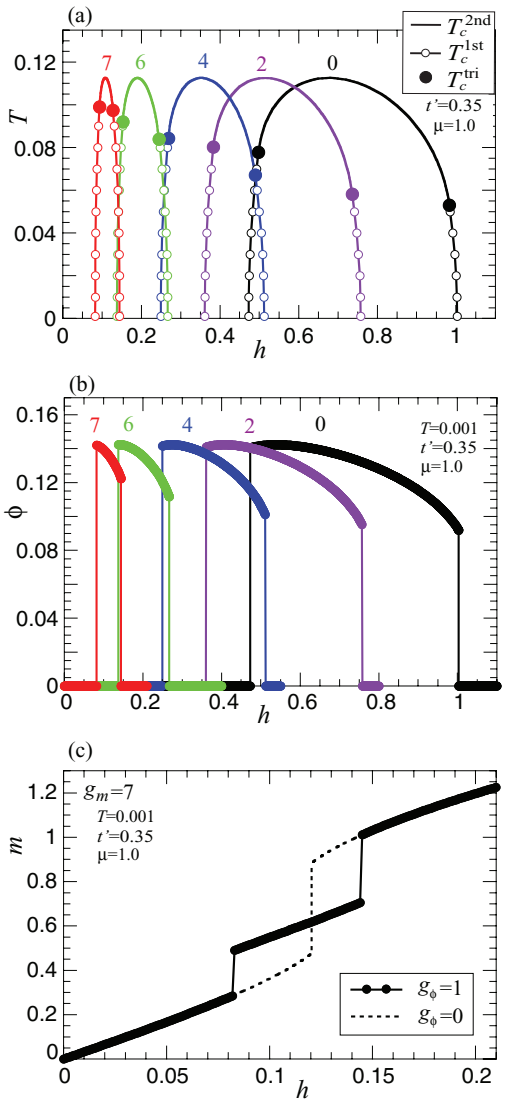

FIG. 7. (Color online) (a) Phase diagram in the (h,T) plane for a sequence of couplings g_m; the value of g_m is indicated near the maximal T_c. The dPI is stabilized inside the dome for each g_m. (b) h dependence of ϕ at $T = 0.001$ for a sequence of g_m. (c) h dependence of m for $g_m = 7$ at $T = 0.001$. The corresponding result for $g_\phi = 0$ is also plotted.

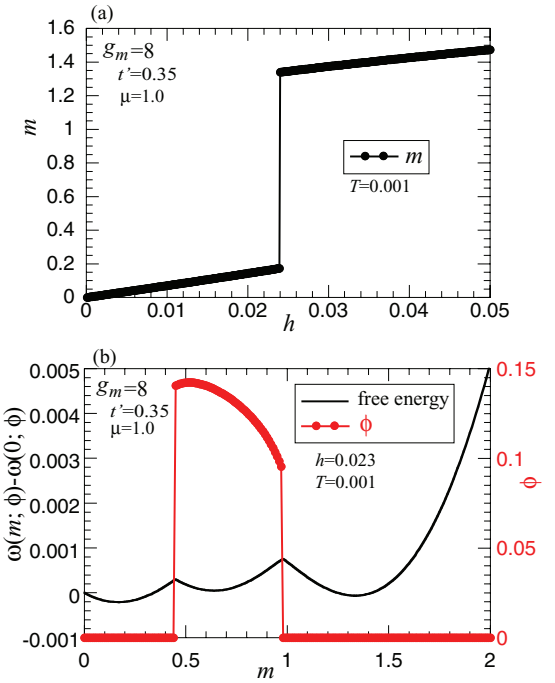

FIG. 8. (Color online) (a) h dependence of m for $g_m = 8$ at $T = 0.001$. (b) Free energy as a function of m at $h = 0.023$ and $T = 0.001$ for $g_m = 8$. The value of ϕ which minimizes the free energy at each m is also plotted.

leading to the same maximal T_c in Fig. 7(a). A similar consideration also explains the same maximal T_c in Figs. 4(b) and 5(b). Keeping in mind that our system is half-metallic in the range of μ where the coexistence is stabilized [see the discussion about Fig. 4(c)] and thus only the down-spin band is active, the coefficient a_2 becomes a function of the quantity $\tilde{\mu} = \frac{-m}{2} + \mu$ for $h = 0$. We confirm the same value of $\tilde{\mu}$ at the maximal T_c in Figs. 4(b) and 5(b), respectively, which necessarily yields the same maximal T_c.

In Fig. 7(b), the order parameter of the dPI is plotted as a function of h for a sequence of g_m at low T. Because of two first-order transitions at low T [Fig. 7(a)], the order parameter exhibits two jumps. Interestingly, the maximal value of ϕ does not depend on g_m. This feature is easily understood from Eqs. (10) and (12). The right-hand side of Eq. (12) depends on the quantity $\tilde{\mu}_{\mathbf{k}\sigma} = \frac{\sigma}{2}(m + h) + d_{\mathbf{k}}\phi$ for a fixed μ. Suppose the maximal value of ϕ, say $\phi_{\max}$, is obtained at $h = h_{\max}$ for $g_m = 0$, namely, for $m = 0$. Even when g_m is turned on, the same value of $\phi_{\max}$ is obtained as long as m and h fulfill the equation

$$m + h = h_{\max}. \tag{22}$$

This equation may hold unless the value of m becomes as large as $h_{\max}$. We can check that Eq. (22) indeed holds up to $g_m \approx 7$, leading to the same maximal value of ϕ for $g_m = 0$–7.

In Fig. 7(c), the magnetization is plotted as a function of h at low T. Because of first-order transitions at low T, the magnetization exhibits two successive jumps. It is instructive to recognize that there could occur a metamagnetic transition at $h \approx 0.12$ if the coupling g_ϕ would be turned off, indicating the underlying competition of the dPI and a metamagnetic transition. We can check that the dPI overcomes the metamagnetic transition up to $g_m = 7.9$.

For $g_m \geqslant 8$, on the other hand, the metamagnetic transition becomes dominant and the magnetization exhibits a single jump as shown in Fig. 8(a). The Landau free energy is plotted in Fig. 8(b) as a function of m at $h = 0.023$, just below the metamagnetic transition; the order parameter ϕ is optimized to minimize the free energy at each m. There are three local minima. Two local minima, where $\phi = 0$ is stabilized, are associated with the metamagnetic phenomenon. The other local minimum, at which ϕ becomes finite, corresponds to a solution of the dPI. This solution, however, does not give the absolute minimum and thus the dPI does not occur. When g_m exceeds 8.25, the FM occurs even for $h = 0$. In this case, neither a metamagnetic transition nor a dPI occurs by applying a magnetic field.

The effect of a ferromagnetic interaction on the dPI for $h \neq 0$ can be summarized as follows: (i) the dPI occurs in a lower magnetic field, (ii) the field range where the dPI is stabilized becomes narrower, (iii) the first-order part of the transition line extends, and (iv) the dPI and a metamagnetic transition compete with each other and the former is realized up to $g_m \approx 8$, and the latter for $8 \lesssim g_m \lesssim 8.25$ for the present choice of parameters.

IV. CONCLUSIONS

We have studied a two-dimensional electron system, where electrons interact with each other via interactions favoring a dPI and FM. In the absence of a magnetic field, we have obtained rich phase diagrams. The dPI and FM typically compete with each other. In fact, while both dPI and FM can be realized simultaneously, they are separated by a first-order phase boundary. Nevertheless, it is possible that the dPI is stabilized inside the FM phase, leading to their coexistence. The presence of t', leading to a breaking of particle-hole symmetry, plays an important role. For $t' = 0$, either the dPI or the FM is typically realized in the plane of the chemical potential and temperature, and coexistence is not stabilized. We have also studied the effect of a magnetic field, motivated by the experimental indication that Sr327 is in the normal state without a magnetic field and exhibits a nematic instability by applying a field. In this case, instead of FM, the dPI competes with a metamagnetic transition. The latter occurs above a threshold strength of the FM interaction and otherwise the dPI is stabilized with a dome-shaped transition line around the van Hove energy in the plane of a field and temperature. With increasing the FM interaction, the center of the dome shifts to a lower field, accompanied by a substantial reduction of the field range where the dPI is stabilized and by an extension of the first-order part of the transition line, although the maximal T_c does not change.

It might seem that the interaction strength of g_m is considered up to a too large value ($g_m \sim 10$) in our study. However, this seemingly large value is due to our definition of g_m in Eq. (5) where a factor of $(1/2)^2$ originating from spin is not absorbed into the definition of g_m.

A typical feature of the dPI is that its mean-field phase diagram is characterized by universal ratios.[21,54] In the model solved in Ref. 54, several universal ratios reasonably agree with experimental values, but ratios of temperature and a magnetic field come out one order of magnitude smaller than the experimental data. For example, in experiments, $T_c^{\rm tri}/h_{\rm tri} \sim 0.6k_B/(0.15\mathfrak{g}\mu_B) = 6\mathfrak{g}^{-1} \approx 3$ if $\mathfrak{g} = 2$, whereas theoretically we obtain $T_c^{\rm tri}/h_{\rm tri} \sim 0.3$ for $g_m = 0$ (Ref. 68); here, $h_{\rm tri}$ is the field at a tricritical point measured from the van Hove energy. However, in the presence of a ferromagnetic interaction, we have found that only the scale of a magnetic field is substantially reduced, while the temperature scale is not. As a result, from Fig. 7(a), we obtain $T_c^{\rm tri}/h_{\rm tri} \sim 2$ and 7 (Ref. 68) for $g_m = 6$ and 7, respectively. The ratio of $T_c^{\rm tri}/h_{\rm tri}$ is substantially modified by a FM interaction to become comparable to the experimental one. The large value of g_m indicates that the system is close to the FM instability for $h = 0$, the same situation as in Sr327.[55–58]

The FM interaction pushes up $T_c^{\rm tri}$ to a higher temperature, but the maximal T_c does not change. As a result, other ratios such as $T_c^{\rm tri}/T_c^{\rm vH}$, where $T_c^{\rm vH}$ is T_c at the van Hove energy, now become slightly larger than the experimental value, although it showed better agreement with experimental data in the model with $g_m = 0$.[54] However, this may be easily improved by invoking weak fluctuations associated with the dPI since it was shown[32,33] that fluctuations suppress $T_c^{\rm tri}$ stronger than $T_c^{\rm vH}$. Therefore, the ratios in the experimental phase diagram of the dPI are well understood by the presence of a FM interaction tuning the system close to the FM instability, and by weak dPI fluctuations.

The lines of first-order phase transitions tilt outward in the experimental phase diagram,[44] indicating that the entropy inside the dPI phase is larger than that in the normal state.[46] This counterintuitive phenomenon is not captured in the present theory. This inconsistency may be explored further in terms of the interplay of ferromagnetic fluctuations and the dPI by going beyond the mean-field model.

Sr327 is a t_{2g} system and band-structure calculations[60,61] show six Fermi surfaces for $h = 0$. The present one-band model focuses on a two-dimensional Fermi surface closest to $\mathbf{k} = (\pi,0)$ and $(0,\pi)$ since such a band contributes to the large density of states near the Fermi energy and thus plays an important role for the dPI and FM instability. It is remarkable that the present simple model captures several features observed in Sr327 and also provides insight into possible fluctuation effects beyond mean-field theory.

On the other hand, we have discarded multiband effects such as the spin-orbit effect, charge transfers among different bands, and detailed features of the electronic band structure in Sr327. There are theoretical studies[4,5] that propose the importance of such multiband effects. Hence, further studies will help to identify the most important physics in Sr327. Actually, orbital nematic order provides another possible scenario.[4,5] Since there are interactions among different orbitals, the dPI is expected to generate orbital nematic order, or vice versa. It is an open question as to which is the driving force for nematicity observed in Sr327.

ACKNOWLEDGMENTS

The author thanks W. Metzner for a critical reading of the manuscript and valuable comments. Support by the Alexander von Humboldt Foundation and a Grant-in-Aid for Scientific Research from Monkasho is also gratefully acknowledged.

[1] P. G. de Gennes and J. Prost, *The Physics of Liquid Crystals* (Clarendon Press, Oxford, UK, 1993).

[2] A. F. Andreev and I. A. Grishchuk, Zh. Eksp. Teor. Fiz. **87**, 467 (1984) [Sov. Phys.-JETP **60**, 267 (1984)].

[3] K. Penc and A. M. Läuchli, in *Introduction to Frustrated Magnetism*, edited by C. Lacroix, P. Mendels, and F. Mila (Springer, Berlin, 2011), p. 331.

[4] S. Raghu, A. Paramekanti, E.-A. Kim, R. A. Borzi, S. A. Grigera, A. P. Mackenzie, and S. A. Kivelson, Phys. Rev. B **79**, 214402 (2009).

[5]W.-C. Lee and C. Wu, Phys. Rev. B **80**, 104438 (2009).
[6]S. Kasahara, H. J. Shi, K. Hashimoto, S. Tonegawa, Y. Mizukami, T. Shibauchi, K. Sugimoto, T. Fukuda, T. Terashima, A. H. Nevidomskyy, and Y. Matsuda, Nature (London) **486**, 382 (2012).
[7]S. Onari and H. Kontani, Phys. Rev. Lett. **109**, 137001 (2012).
[8]S. A. Kivelson, E. Fradkin, and V. J. Emery, Nature (London) **393**, 550 (1998).
[9]H. Yamase and H. Kohno, J. Phys. Soc. Jpn. **69**, 332 (2000); **69**, 2151 (2000).
[10]C. J. Halboth and W. Metzner, Phys. Rev. Lett. **85**, 5162 (2000).
[11]I. J. Pomeranchuk, J. Exptl. Theoret. Phys. (U.S.S.R.) **35**, 524 (1958) [Sov. Phys.-JETP **8**, 361 (1959)].
[12]A. Miyanaga and H. Yamase, Phys. Rev. B **73**, 174513 (2006).
[13]B. Edegger, V. N. Muthukumar, and C. Gros, Phys. Rev. B **74**, 165109 (2006).
[14]M. Bejas, A. Greco, and H. Yamase, Phys. Rev. B **86**, 224509 (2012).
[15]I. Grote, E. Körding, and F. Wegner, J. Low Temp. Phys. **126**, 1385 (2002); V. Hankevych, I. Grote, and F. Wegner, Phys. Rev. B **66**, 094516 (2002).
[16]A. Neumayr and W. Metzner, Phys. Rev. B **67**, 035112 (2003).
[17]S. Okamoto, D. Sénéchal, M. Civelli, and A.-M. S. Tremblay, Phys. Rev. B **82**, 180511 (2010).
[18]S.-Q. Su and T. A. Maier, Phys. Rev. B **84**, 220506(R) (2011).
[19]J. Buenemann, T. Schickling, and F. Gebhard, Europhys. Lett. **98**, 27006 (2012).
[20]I. Khavkine, C.-H. Chung, V. Oganesyan, and H.-Y. Kee, Phys. Rev. B **70**, 155110 (2004).
[21]H. Yamase, V. Oganesyan, and W. Metzner, Phys. Rev. B **72**, 035114 (2005).
[22]J. Quintanilla and A. J. Schofield, Phys. Rev. B **74**, 115126 (2006).
[23]J. Quintanilla, M. Haque, and A. J. Schofield, Phys. Rev. B **78**, 035131 (2008).
[24]C. A. Lamas, D. C. Cabra, and N. Grandi, Phys. Rev. B **78**, 115104 (2008).
[25]M. V. Zverev, J. W. Clark, Z. Nussinov, and V. A. Khodel, Phys. Rev. B **82**, 125111 (2010).
[26]V. Oganesyan, S. A. Kivelson, and E. Fradkin, Phys. Rev. B **64**, 195109 (2001).
[27]D. G. Barci and L. E. Oxman, Phys. Rev. B **67**, 205108 (2003).
[28]J. Nilsson and A. H. Castro Neto, Phys. Rev. B **72**, 195104 (2005).
[29]M. J. Lawler, D. G. Barci, V. Fernández, E. Fradkin, and L. Oxman, Phys. Rev. B **73**, 085101 (2006).
[30]M. Zacharias, P. Wölfle, and M. Garst, Phys. Rev. B **80**, 165116 (2009).
[31]D. L. Maslov and A. V. Chubukov, Phys. Rev. B **81**, 045110 (2010).
[32]P. Jakubczyk, W. Metzner, and H. Yamase, Phys. Rev. Lett. **103**, 220602 (2009).
[33]H. Yamase, P. Jakubczyk, and W. Metzner, Phys. Rev. B **83**, 125121 (2011).
[34]W. Metzner, D. Rohe, and S. Andergassen, Phys. Rev. Lett. **91**, 066402 (2003).
[35]L. Dell'Anna and W. Metzner, Phys. Rev. B **73**, 045127 (2006).
[36]H. Yamase and W. Metzner, Phys. Rev. Lett. **108**, 186405 (2012).
[37]V. Hinkov, S. Pailhès, P. Bourges, Y. Sidis, A. Ivanov, A. Kulakov, C. T. Lin, D. Chen, C. Bernhard, and B. Keimer, Nature (London) **430**, 650 (2004).
[38]V. Hinkov, P. Bourges, S. Pailhès, Y. Sidis, A. Ivanov, C. D. Frost, T. G. Perring, C. T. Lin, D. P. Chen, and B. Keimer, Nat. Phys. **3**, 780 (2007).
[39]V. Hinkov, D. Haug, B. Fauqué, P. Bourges, Y. Sidis, A. Ivanov, C. Bernhard, C. T. Lin, and B. Keimer, Science **319**, 597 (2008).
[40]H. Yamase and W. Metzner, Phys. Rev. B **73**, 214517 (2006).
[41]H. Yamase, Phys. Rev. B **79**, 052501 (2009).
[42]R. Daou, J. Chang, D. LeBoeuf, O. Cyr-Choinière, F. Laliberté, N. Doiron-Leyraud, B. J. Ramshaw, R. Liang, D. A. Bonn, W. H. Hardy, and L. Taillefer, Nature (London) **463**, 519 (2010).
[43]A. Hackl and M. Vojta, Phys. Rev. B **80**, 220514(R) (2009).
[44]S. A. Grigera, P. Gegenwart, R. A. Borzi, F. Weickert, A. J. Schofield, R. S. Perry, T. Tayama, T. Sakakibara, Y. Maeno, A. G. Green, and A. P. Mackenzie, Science **306**, 1154 (2004).
[45]R. A. Borzi, S. A. Grigera, J. Farrell, R. S. Perry, S. J. S. Lister, S. L. Lee, D. A. Tennant, Y. Maeno, and A. P. Mackenzie, Science **315**, 214 (2007).
[46]A. W. Rost, R. S. Perry, J.-F. Mercure, A. P. Mackenzie, and S. A. Grigera, Science **325**, 1360 (2009).
[47]H.-Y. Kee and Y. B. Kim, Phys. Rev. B **71**, 184402 (2005).
[48]H. Doh, Y. B. Kim, and K. H. Ahn, Phys. Rev. Lett. **98**, 126407 (2007).
[49]C. Puetter, H. Doh, and H.-Y. Kee, Phys. Rev. B **76**, 235112 (2007).
[50]H. Yamase, Phys. Rev. Lett. **102**, 116404 (2009); Phys. Rev. B **80**, 115102 (2009).
[51]A. F. Ho and A. J. Schofield, Europhys. Lett. **84**, 27007 (2008).
[52]M. H. Fischer and M. Sigrist, Phys. Rev. B **81**, 064435 (2010).
[53]H. Yamase and A. A. Katanin, J. Phys. Soc. Jpn. **76**, 073706 (2007); **79**, 127001 (2010).
[54]H. Yamase, Phys. Rev. B **76**, 155117 (2007).
[55]S.-I. Ikeda, Y. Maeno, S. Nakatsuji, M. Kosaka, and Y. Uwatoko, Phys. Rev. B **62**, R6089 (2000).
[56]S.-I. Ikeda, N. Shirakawa, T. Yanagisawa, Y. Yoshida, S. Koikegami, S. Koike, M. Kosaka, and Y. Uwatoko, J. Phys. Soc. Jpn. **73**, 1322 (2004).
[57]L. Capogna, E. M. Forgan, S. M. Hayden, A. Wildes, J. A. Duffy, A. P. Mackenzie, R. S. Perry, S. Ikeda, Y. Maeno, and S. P. Brown, Phys. Rev. B **67**, 012504 (2003).
[58]K. Kitagawa, K. Ishida, R. S. Perry, T. Tayama, T. Sakakibara, and Y. Maeno, Phys. Rev. Lett. **95**, 127001 (2005).
[59]P. Gegenwart, F. Weickert, M. Garst, R. S. Perry, and Y. Maeno, Phys. Rev. Lett. **96**, 136402 (2006).
[60]I. Hase and Y. Nishihara, J. Phys. Soc. Jpn. **66**, 3517 (1997).
[61]D. J. Singh and I. I. Mazin, Phys. Rev. B **63**, 165101 (2001).
[62]A. J. Millis, A. J. Schofield, G. G. Lonzarich, and S. A. Grigera, Phys. Rev. Lett. **88**, 217204 (2002).
[63]B. Binz and M. Sigrist, Europhys. Lett. **65**, 816 (2004).
[64]A. M. Berridge, Phys. Rev. B **83**, 235127 (2011).
[65]R. S. Perry, L. M. Galvin, S. A. Grigera, L. Capogna, A. J. Schofield, A. P. Mackenzie, M. Chiao, S. R. Julian, S. I. Ikeda, S. Nakatsuji, Y. Maeno, and C. Pfleiderer, Phys. Rev. Lett. **86**, 2661 (2001).
[66]B. Valenzuela and M. A. H. Vozmediano, Phys. Rev. B **63**, 153103 (2001).
[67]M. H. Fischer, and E.-A. Kim, Phys. Rev. B **84**, 144502 (2011).
[68]We have taken an average of two different ratios of $T_c^{\rm tri}/h_{\rm tri}$ because of the presence of two tricritical points.